AGU ADVANCING EARTH AND SPACE SCIENCES

Geophysical Research Letters

RESEARCH LETTER
10.1029/2025GL119632

Statistical Characteristics of Stormtime Bursty Bulk Flows

Anusree P. Devanandan[1], Amy Keesee[1,2], Savvas Raptis[3], Shinichi Ohtani[3], Viacheslav Merkin[3], and Matina Gkioulidou[3]

[1]Department of Physics and Astronomy, University of New Hampshire, Durham, NH, USA, [2]Space Science Center, University of New Hampshire, Durham, NH, USA, [3]Johns Hopkins University Applied Physics Laboratory, Laurel, MD, USA

Key Points:

- Convection electric field E_y, within bursty bulk flows (BBFs) is enhanced during stormtime compared to non-storm times
- This enhancement is due to an elevated northward magnetic field B_z in plasmasheet, while BBF velocity stays similar to non-storm times
- During storm and non-storm times, BBF E_y enhancement over background is mainly due to their higher velocity, not higher B_z

Supporting Information:

Supporting Information may be found in the online version of this article.

Correspondence to:

A. P. Devanandan,
ap1440@usnh.edu

Citation:

Devanandan, A. P., Keesee, A., Raptis, S., Ohtani, S., Merkin, V., & Gkioulidou, M. (2026). Statistical characteristics of stormtime bursty bulk flows. *Geophysical Research Letters*, *53*, e2025GL119632. https://doi.org/10.1029/2025GL119632

Received 7 OCT 2025
Accepted 24 JAN 2026

Author Contributions:

Conceptualization: Savvas Raptis
Data curation: Anusree P. Devanandan, Savvas Raptis
Formal analysis: Anusree P. Devanandan
Funding acquisition: Amy Keesee, Viacheslav Merkin
Methodology: Amy Keesee, Savvas Raptis, Shinichi Ohtani, Viacheslav Merkin, Matina Gkioulidou
Project administration: Amy Keesee, Viacheslav Merkin
Supervision: Amy Keesee
Visualization: Anusree P. Devanandan
Writing – original draft: Anusree P. Devanandan

Abstract Bursty bulk flows (BBFs) play a significant role in transporting plasma earthward in the magnetotail. While their properties have been extensively studied, their behavior during geomagnetic storms needs further understanding. In this study, we investigate the stormtime characteristics of BBFs, and compare them to non-stormtime, by performing a superposed epoch analysis using data from ISAS/NASA's Geotail mission. Our results show that the properties of BBFs during stormtime and non-stormtime remain largely consistent relative to the background plasma sheet conditions. The convection electric field is higher for stormtime BBFs which is primarily associated with an elevated magnetic field in the plasma sheet during storms. Moreover, stormtime plasma sheet conditions, such as an enhanced magnetic field and an elevated ion temperature, are reflected in the properties of BBFs indicating the strong influence of the background plasma environment on BBF dynamics.

Plain Language Summary Solar activity, such as eruptions and fast solar wind streams, can disturb the Earth's magnetic field and the surrounding space environment, producing geomagnetic storms. These storms can affect satellites, navigation systems, and power grids. In the nightside of the Earth's space environment there are fast, short-lived jets of charged particles, called bursty bulk flows (BBFs), which carry mass and energy toward the Earth. The characteristics of these flows have been studied for decades, but their behavior during geomagnetic storms is not fully understood. In this study, we used data from the ISAS/NASA's Geotail spacecraft to study BBFs during storms and compare their properties with those during non-storm times. We found that while the basic nature of BBFs is similar in both cases, stormtime BBFs occur in an environment with stronger magnetic fields and hotter plasma. These background conditions strongly influence the properties of BBFs and how they behave during storms, leading to the transport of more magnetic flux during storms compared to non-storm times.

1. Introduction

High speed flow bursts, a specific kind of which are called bursty bulk flows (BBFs), are fast (a few hundred km/s), transient (a few minutes) plasma flows within the magnetotail plasma sheet and play a central role in transporting mass, momentum, and energy earthward (Angelopoulos et al., 1992; Baumjohann & Paschmann, 1990; Fu et al., 2011). Observations suggest that BBFs are responsible for a significant fraction of energy transport earthward from the reconnection site (Angelopoulos et al., 1992, 1994; Runov et al., 2011). They also play a major role in the ring current build-up by transporting energy, magnetic flux and plasma from the magnetotail into the inner magnetosphere (Sciola et al., 2023; Yang et al., 2015). While it is well established that BBFs play a significant role in plasma sheet convection, the extent of their contribution specifically to convection during stormtime remains largely unexplored.

Several studies primarily using in situ observations have been conducted to characterize these fast flows such as their spatial and temporal scale, structure, shape of flow channels, etc., (Angelopoulos et al., 1997; Nakamura, Amm, et al., 2005; Nakamura, Baumjohann, et al., 2005; Ohtani et al., 2004; Sitnov et al., 2019). Some of the key observed features of BBFs include a sharp increase in the northward magnetic field (B_z), called a dipolarization front, elevated ion temperatures and energetic particle fluxes, and a reduction in plasma pressure and density. Global magnetohydrodynamic (MHD) simulations have also been conducted to investigate the origin and evolution of mesoscale flows in the magnetotail. These simulations reproduce the key features that show good agreement with the observed properties of BBFs (Merkin et al., 2019; Ohtani et al., 2004; Wiltberger et al., 2015).

Writing – review & editing:
Amy Keesee, Savvas Raptis, Shinichi Ohtani, Viacheslav Merkin, Matina Gkioulidou

Plasma sheet properties such as composition, particle dynamics and magnetic field structure change during stormtime compared to non-stormtime (Hori et al., 2005; Juusola et al., 2011; Ohtani & Mukai, 2008; Raptis et al., 2024). It is unclear how these changes in the plasma sheet conditions during geomagnetic storms affect the characteristics of BBFs. Previous work has shown that during storms the plasma sheet exhibits an elevated convection electric field (E_y), correlated with an increase in equatorial B_z and only small variations in earthward $V_{\perp x}$ compared to non-storm periods (Ohtani & Mukai, 2008; Raptis et al., 2024). However, the contribution of BBFs to this stormtime plasmasheet behavior remains unclear. In this study, we investigate the stormtime characteristics of BBFs through a superposed epoch analysis using data from ISAS/NASA's Geotail spacecraft. Specifically, we focus on examining how storm-driven changes in the plasma sheet environment, such as elevated convection electric fields and stronger magnetic fields, affect BBF properties. The details of the data selection and methodology are described in Section 2. In Section 3, we discuss the observed properties of BBFs from a superposed epoch analysis, and the results are summarized in the last section (Section 4).

2. Data and Methodology

Data from the ISAS/NASA Geotail mission (1992–2022) are used for this study (Nishida, 1994). Magnetic field data are obtained from the magnetic field experiment (MGF) instrument, and plasma parameters and moments are calculated from the low-energy plasma experiment (LEP) instrument on Geotail. The data used in this study have a temporal resolution of 12 s, and we used Aberrated Geocentric Solar Magnetospheric (AGSM) coordinate system for our analysis. Due to Earth's orbital motion around the Sun, the solar wind does not arrive strictly along the Sun-Earth line. This relative motion causes an aberration of a few degrees resulting in a solar wind flow direction that is slightly inclined with respect to the radial direction. To account for this, we used GSM coordinates aberrated by 4°. The earthward magnetic flux transport can be quantified by measuring the strength of the convection electric field E_y; however the electric field data from Geotail has been unavailable since February 2007. Previous studies have shown that $(-\mathbf{V} \times \mathbf{B})_y$ is very well correlated to the measured E_y (Kasaba et al., 2006; Ohtani & Mukai, 2008; Raptis et al., 2024). Since $(-\mathbf{V} \times \mathbf{B})_y$ is available for the entire Geotail data set and is a good proxy for E_y, we use it to quantify the convection electric field for our analyses.

A list of earthward BBFs were created from the entire available Geotail data set (1994–2022). BBF events in the plasma sheet were identified using the x-component of the velocity perpendicular to the local magnetic field ($V_{\perp x}$). The selection criteria that we adopted are similar to Ohtani et al. (2004) but with a lower threshold value for $V_{\perp x}$. For a BBF event, the $V_{\perp x}$ must remain above 100 km/s throughout the entire interval, with at least one point reaching a peak value of 250 km/s or higher. The ion beta (β_i), which is the ratio of the ion thermal pressure to the magnetic pressure, has to be greater than 0.5 during each event. This condition ensures that the spacecraft is within the plasma sheet region during the event. For all the selected intervals, the spacecraft is required to be within $\pm 15\ R_E$ in $Y_{GSM,4^\circ}$ and -15 to $-31\ R_E$ in $X_{GSM,4^\circ}$, where the subscript $GSM, 4^\circ$ denotes the GSM coordinate aberrated by 4°. In addition to this, the ion density is required to be less than 5 cm^{-3}. This criterion removes any potential measurements from the magnetosheath region. Our BBF selection criteria differ slightly from those of Angelopoulos et al. (1992): we used $V_{\perp x}$ rather than V_x, and applied a lower velocity threshold to account for the deceleration of flows closer to Earth. Additionally, we do not include any criteria to define the burstiness of the flows. However, because our analysis window extends tens of minutes, it should capture not only the initial fast flow but also the subsequent flows and therefore our intervals consist of what are typically referred to as BBFs. The selected BBF intervals are separated into three categories, those occurring during storm main phase, storm recovery phase, and non-stormtime intervals. To identify and classify storm intervals into main and recovery phases we used the openly available list generated in Raptis et al. (2024). To generate this list, SuperMAG Ring Current (SMR) index was used to define and identify storm intervals. For a storm to be registered in the data set, SMR is required to drop to −50 nT. Any interval that was not identified as a stormtime interval is considered to be in non-stormtime conditions. The list of geomagnetic storms from 1993 to 2025 and their classification into main and recovery phases can be accessed from Raptis et al. (2024) or from the Data Availability Statement below.

To study the temporal characteristics of BBFs during storms, we performed a superposed epoch analysis (SEA) on the magnetic field and plasma parameters for the selected stormtime and non-stormtime BBF events. The total duration of the SEA was taken to be 20 min with the zero epoch defined as the last point with $V_{\perp x} < 150$ km/s

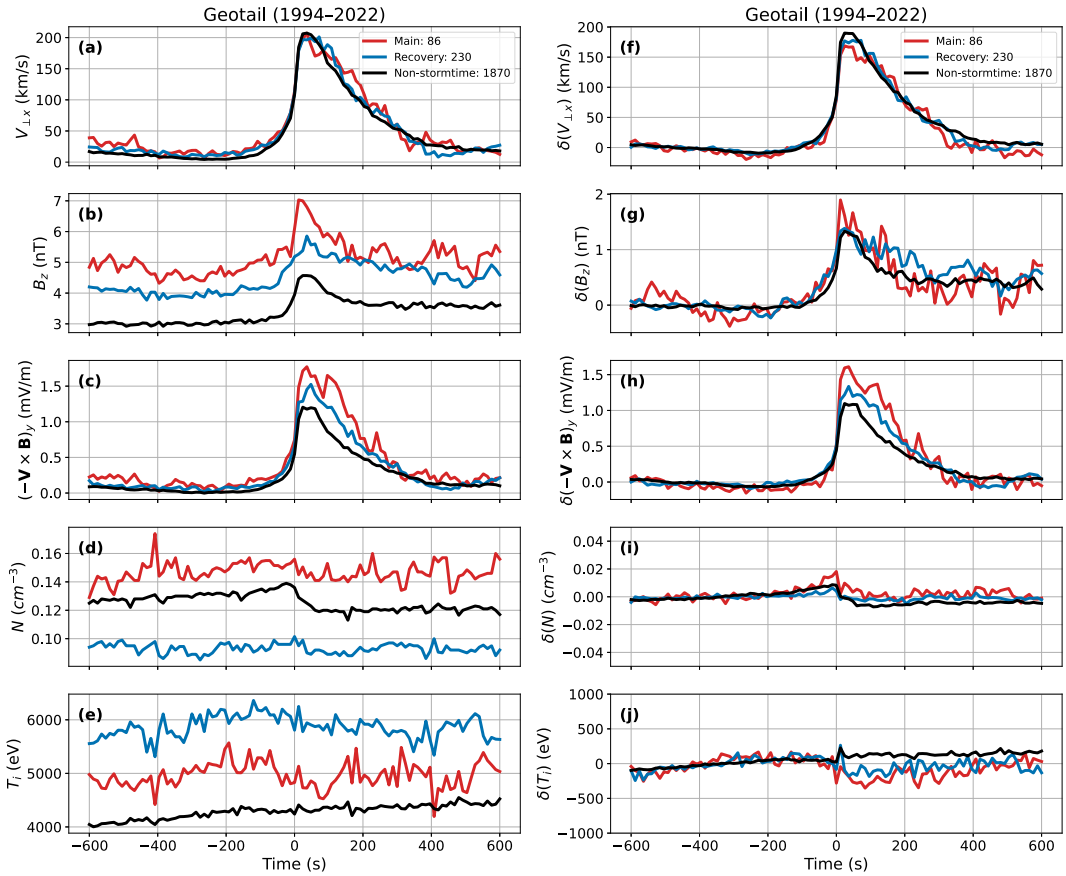

Figure 1. Superposed Epoch Analysis (SEA) of BBFs measured by Geotail during 1994–2022. The median of each parameter is plotted for BBF intervals for the main phase (red), recovery phase (blue) and non-stormtime (black). Panel (a) shows the velocity component perpendicular to the magnetic field, $V_{\perp x}$, in km/s, (b) shows the z component of magnetic field B_z in nT, (c) is the median values of convection electric field, $(-\mathbf{V}\times\mathbf{B})_y$ in (mV/m), (d) shows the ion density in $\left(\mathrm{cm}^{-3}\right)$, and (e) is the median values of ion temperature in eV. Panels (f–j) show the corresponding median values after subtracting the background plasma sheet values.

before exceeding 250 km/s. We ensure that there are no BBF intervals during the preceding 5 min from the zero epoch to avoid statistical contamination of the SEA by secondary events. In addition, β_i is required to be greater than 0.5 for 5 min before and after the zero epoch. A total of 2186 BBF intervals satisfy all the above criteria and are used for our analysis. These intervals are separated into stormtime and non-stormtime intervals with 86 found during main phase, 230 during recovery phase, and 1870 during non-stormtime. In all the figures, the main phase, the recovery phase, and the non-stormtime intervals are represented in red, blue, and black, respectively. The location of the spacecraft during each BBF event at the zero epoch in the GSM x-y plane is provided in the Supporting Information S1 (Figure S1). It should be noted that many of the BBF events identified in our data set are located at the dawnside (Figure S1 in Supporting Information S1).

3. Results

3.1. Magnetic Field and Plasma Parameters

A superposed epoch analysis has been performed on the selected BBF intervals to investigate their stormtime characteristics. Figure 1 shows the median superposed values of the magnetic field and the plasma parameters during the main phase (red), recovery phase (blue), and non-stormtime (black). $V_{\perp x}$ (Figure 1a) increases sharply around the zero epoch for BBFs during all phases. The median values of $V_{\perp x}$ are nearly identical, with no observed

difference in the statistical behavior of $V_{\perp x}$ between the BBFs during stormtime and non-stormtime suggesting that the flow velocity is comparable throughout the epoch window for both stormtime and non-stormtime BBFs.

A dipolarization of the magnetic field, indicated by an increase in B_z (z component of the local magnetic field) is observed at the zero epoch for all BBF intervals regardless of their phase characterization. This is one of the common observed features of BBFs. For stormtime BBFs, B_z is elevated throughout the epoch window, with the main phase having a higher B_z compared to the recovery phase and non-stormtime (Figure 1b). The increase in B_z during stormtime is consistent with an enhanced magnetic field in the plasma sheet observed during storms (Ohtani & Mukai, 2008; Raptis et al., 2024). The convection electric field, $(-\mathbf{V} \times \mathbf{B})_y$, shown in Figure 1 in panel (c), increases sharply around zero epoch and eventually drops to the background value in a few minutes as the velocity drops to its initial value. This indicates an elevated magnetic flux transport in the plasma sheet after the start of a BBF event. Notably, $(-\mathbf{V} \times \mathbf{B})_y$ is larger during the main phase compared to the recovery phase and non-stormtime BBFs at the zero epoch and remains elevated for a few minutes afterward. This feature may be due to an elevated magnetic field and/or an increase in $V_{\perp x}$ during the main phase of the storm, a point further analyzed in the Section 3.2.

Although an increase in ion temperature and a drop in ion density are observed after the zero epoch for non-stormtime BBF intervals, this trend is not apparent during the main phase and recovery phase (Figures 1d and 1e). This may be a result of the lower number of events during stormtime, reducing the ability to statistically observe the temporal variations of these parameters. We therefore examined a few individual events, but did not observe any clear trend in ion temperature or density for events during the main or the recovery phase. This may potentially suggest a different behavior between non-stormtime and stormtime events. Further investigation is needed to address this, requiring more observations to improve statistical confidence. When recovery phase intervals are compared to the main phase and non-stormtime intervals, the median values of ion density are lower, and the ion temperature is elevated throughout the entire epoch window. To further investigate this, we separated the stormtime BBF intervals into those driven by high-speed solar wind stream (HSS) and those driven by interplanetary coronal mass ejections (ICME) based on the list of storms identified by Pinto et al. (2022), which was expanded and classified by storm type by Marchezi and Pinto (2025). We excluded BBF events during storms that were driven by both ICME and HSS and included only those intervals that were driven exclusively by either an ICME or an HSS. For the selected BBF intervals during HSS- and ICME-driven storms, we performed a superposed epoch analysis of ion temperature and ion density. The SEA of density and ion temperature of BBF intervals during HSS-driven storms and ICME-driven storms is shown in Figure S2 in Supporting Information S1. While density and temperature exhibit slight variation between the main and recovery phase BBF intervals during ICME-driven storms, a clear difference is observed in HSS-driven storms, where recovery phase BBFs show lower densities and higher temperatures compared to those during the main phase. Therefore, the characteristics of ion density and ion temperature observed during the recovery phase in the original SEA (Figures 1d and 1e) may be predominantly influenced by events associated with HSS-driven storms. Since only limited number of BBF intervals were identified during HSS- and ICME-driven storms, this result may not be statistically true for all cases. Alternatively, a dawn-dusk asymmetry in the plasma sheet ion temperature could have also contributed to this picture (Wang et al., 2012). To identify which of these factors is the primary cause, a more detailed analysis is needed and is out of the scope of this letter. The locations of these BBF intervals at zero epoch in the GSM x-y plane are shown in Figure S3 in Supporting Information S1.

In addition, to investigate the relative changes associated with BBFs and isolate their contribution, we performed a third superposed epoch analysis after subtracting the background plasma sheet values. We calculate the background plasma sheet values by taking the mean of each parameter from 600 to 204 s before the zero epoch. The velocity is near zero at 204 s before the zero epoch, allowing us to calculate the properties of the background plasma sheet prior to the onset of BBFs. The median of the superposed values are shown in Figure 1, panels (f)–(j). This analysis confirmed the picture shown in Figure 1 panels (a)–(e) that BBFs follow similar trends during stormtime and non-stormtime and the observed differences arise from the background plasma sheet conditions. Specifically, $V_{\perp x}$ (Figure 1f) values are very similar for stormtime and non-stormtime BBFs, and B_z and ion density (Figure 1, panels (g) and (i)) show minimal variation (less than 10%) between the main phase, recovery phase, and non-stormtime intervals. Ion temperature (Figure 1j) decreases after the flow for stormtime events, while remaining elevated for non-stormtime events. However, a more detailed analysis is necessary to address the statistical robustness of this finding and its origin. Although all other parameters exhibit minimal

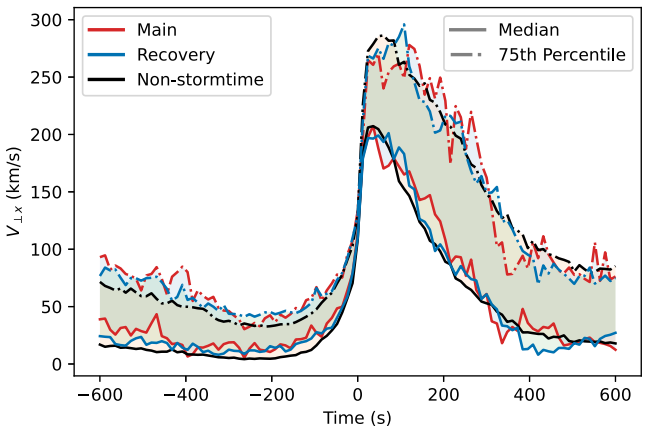

Figure 2. Median and 75th percentile of the superposed values of $V_{\perp x}$ (in km/s) of BBFs during main phase (red), recovery phase (blue) and non-stormtime (black).

variations, $(-\mathbf{V} \times \mathbf{B})_y$ (Figure 1h) is observed to be elevated at the zero epoch for stormtime BBFs. A detailed analysis of $(-\mathbf{V} \times \mathbf{B})_y$ is presented in the following subsection to further explore this enhanced magnetic flux transport during stormtime BBFs.

Finally, to ensure that the similarity in the values of $V_{\perp x}$ observed between the stormtime and non-stormtime BBFs in the SEA is not merely a consequence of using median values, we plotted both the median and the 75th percentile of $V_{\perp x}$ for the main phase, recovery phase, and non-stormtime (Figure 2). It is clear from Figure 2 that the velocity profiles are nearly identical for BBFs occurring during both stormtime and non-stormtime even when examining the values toward the top quartile of the distribution. This confirms that the velocity profiles are similar between stormtime and non-stormtime BBFs.

3.2. Magnetic Flux Transport

In order to investigate the relative contribution of the magnetic field and velocity changes toward the increased convection electric field, we performed a superposed epoch analysis on the components of change in $(-\mathbf{V} \times \mathbf{B})_y$:

$$\begin{aligned}\delta(-\mathbf{V}\times\mathbf{B})_y &= \delta\left(V_xB_z - V_zB_x\right)\\ &= \delta V_x\cdot B_z + V_x\cdot\delta B_z + \delta V_x\cdot\delta B_z - \left(\delta V_z\cdot B_x + V_z\cdot\delta B_x + \delta V_z\cdot\delta B_x\right)\end{aligned} \tag{1}$$

where $\delta(-\mathbf{V} \times \mathbf{B})_y$ is the total change in the convection electric field (Figure 1h), δV_x, δV_z, δB_x, δB_z represent the deviations from their mean values 600 to 204 s before the zero epoch, and V_x, V_z, B_x, B_z are the corresponding mean background plasma sheet values, calculated in the same manner as described in Section 3.1. The contributions of the terms $\delta V_z \cdot B_x$, $V_z \cdot \delta B_x$ and $\delta V_z \cdot \delta B_x$ to the change in $(-\mathbf{V} \times \mathbf{B})_y$ were found to be negligible and therefore are omitted from our analysis (Figure S4 in Supporting Information S1). Figure 3 shows the median of the superposed values for each remaining term in Equation 1, that is, $\delta(-\mathbf{V} \times \mathbf{B})_y = \delta V_x \cdot B_z + V_x \cdot \delta B_z + \delta V_x \cdot \delta B_z$. Panel a (Figure 3) shows the total change in the convection electric field while panels b, c, and d represent the individual contributing terms. Although both changes in the velocity and the magnetic field contribute to the overall change in the convection electric field, the contribution from $\delta V_x \cdot B_z$ (Figure 3b) is higher compared to the other terms. This suggests that for BBFs, velocity changes interacting with the local background magnetic field have a dominant contribution to the increase in the convection electric field. The contribution from the term $V_x \cdot \delta B_z$ is negligible compared to the other terms showing that the relative increase in $(-\mathbf{V} \times \mathbf{B})_y$ is associated primarily with increased BBF velocities and an elevated background magnetic field, rather than the dipolarization of B_z. Furthermore, BBFs observed during main phase exhibit a larger increase in the convection electric field after the zero epoch than those during the recovery phase or non-stormtime. This difference is associated with an elevated magnetic field during stormtime. Median values were used for this analysis to minimize the effect of outliers, and therefore the sum of the contributing terms does not necessarily equal the total change in $(-\mathbf{V} \times \mathbf{B})_y$. A similar analysis using the mean values is presented in the Supporting Information S1 (Figure S5). In this case, the sum of terms is equal to the total change in $(-\mathbf{V} \times \mathbf{B})_y$, while the overall relative contribution between each term remains the same.

Finally, to quantify how the contribution of BBFs to the magnetic flux transport varies between stormtime and non-stormtime intervals, we computed the average magnetic flux per unit width across the flow channel in the GSM y direction, from the superposed data, by time integrating the convection electric field and taking its mean value that is,

$$\overline{\Phi} = \frac{1}{N}\sum_{i=1}^{N}\left(\sum_{t=t_0}^{t_1}\left[(-\mathbf{V}(t)\times\mathbf{B}(t))_y\,\Delta t\right]\right), \tag{2}$$

where $\overline{\Phi}$ is the average magnetic flux per unit width across the flow channel, N is the number of events, and $\Delta t = 12$ s is the data resolution. The summation limits (t_0, t_1) corresponds to $(-408, -204)$ s (background plasma

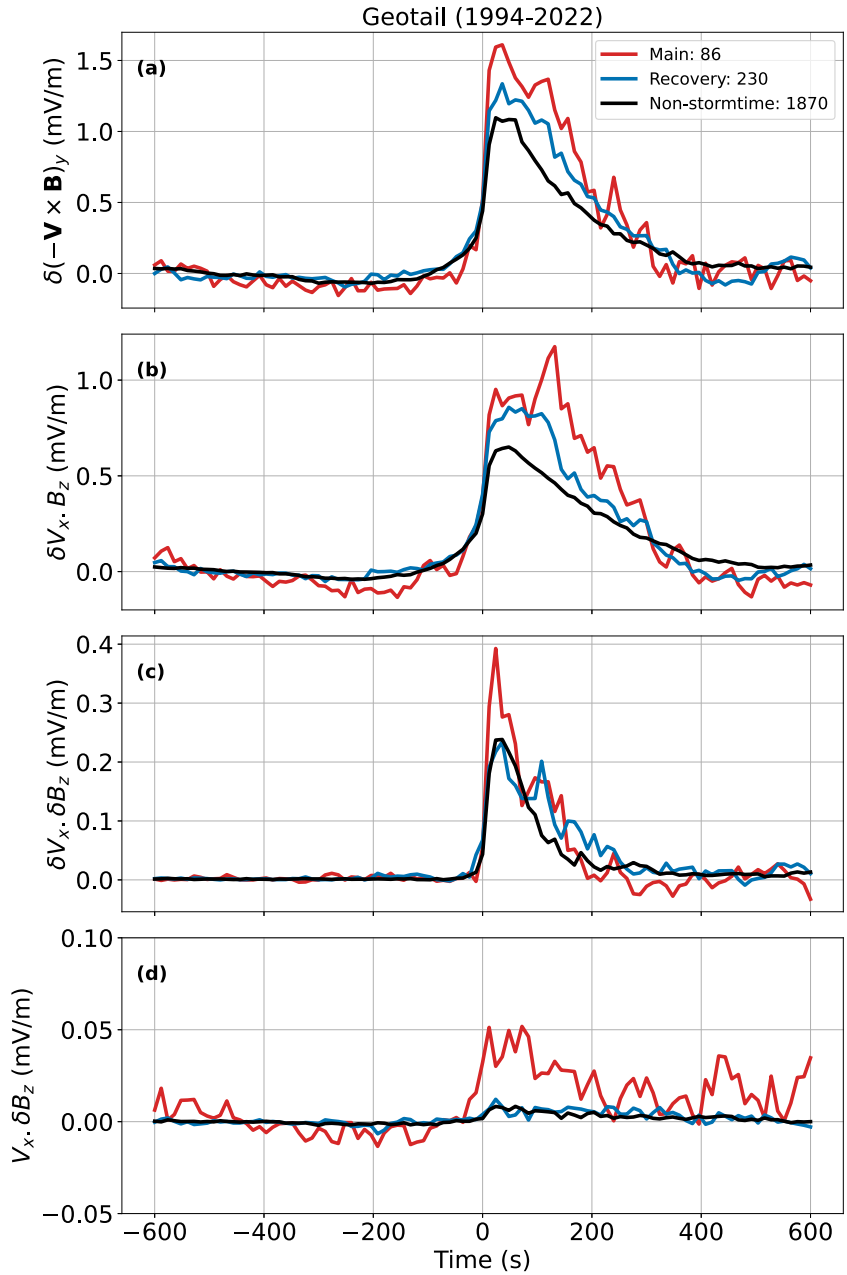

Figure 3. Median of superposed values of the components of the expression $\delta(-\mathbf{V}\times\mathbf{B})_y = \delta V_x\cdot B_z + V_x\cdot\delta B_z + \delta V_x\cdot\delta B_z$ for main phase (red), recovery phase (blue) and non-stormtime (black). (a) is the median of superposed values of the total change in the convection electric field, $(-\mathbf{V}\times\mathbf{B})_y$ (mV/m) and all other panels indicate the median of superposed values of contributing terms of the equation as follows: (b) $\delta V_x\cdot B_z$ (mV/m) (c) $\delta V_x\cdot\delta B_z$ (mV/m) and (d) $V_x\cdot\delta B_z$ (mV/m).

sheet values, $\overline{\Phi}_{PS}$) and (0, 204) s (after the zero epoch, $\overline{\Phi}_{BBF}$) respectively (Table 1). Compared to non-stormtime and the recovery phase, $\overline{\Phi}$ is higher during the main phase both before the onset of BBF (i.e., before −204s) and after the zero epoch. However, the ratio of $\overline{\Phi}$ after the zero epoch to before the onset of BBF, $\overline{\Phi}_{BBF}/\overline{\Phi}_{PS}$, is lower during the main phase than during recovery or non-storm periods. This is likely because the BBF dipolarizations (δB_z) are similar across phases (Figure 1g), making the relative jump smaller in the main phase during which the background plasma sheet B_z is already elevated.

Table 1
Magnetic Flux per Unit Width Across the Flow Channel for BBFs During Main Phase, Recovery Phase and Non-Stormtime for the Background Plasma Sheet $(\overline{\Phi}_{PS})$ *and BBFs* $(\overline{\Phi}_{BBF})$

Phase	Background plasma sheet, $\overline{\Phi}_{PS}$ (mWb/m)	BBF, $\overline{\Phi}_{BBF}$ (mWb/m)
Main Phase	36.062	370.732
Recovery Phase	15.591	283.831
Non-stormtime	6.292	243.807

4. Summary and Discussion

In this study, we conducted a superposed epoch analysis of BBFs to investigate their characteristics during stormtime and compared them to the non-stormtime properties. We showed that, when the mean background plasma sheet values are subtracted, BBF properties are comparable between stormtime and non-stormtime conditions (Figure 1 panels (f)–(j)). However, there is more variability during the main phase of the storm. Since this variability is relatively small (<10% compared to background level) and the statistical sample is relatively low, a more detailed analysis is needed to assess the robustness of these differences. The quartile distribution of the flow velocity, $V_{\perp x}$, shows that $V_{\perp x}$ have similar values during stormtime and non-stormtime (Figure 2). Similar values for $V_{\perp x}$ are expected at the zero epoch as a result of the criteria used for defining the zero epoch. However, the SEA (Figure 1a) and quartile distribution of $V_{\perp x}$ (Figure 2) indicate that the flow velocity is comparable throughout the epoch window, across all three sets of intervals, with the exception of a slightly higher flow velocity following the zero epoch during main-phase intervals. The stormtime plasma sheet is characterized by an enhanced B_z and an elevated convection electric field $(-\mathbf{V} \times \mathbf{B})_y$ (Hori et al., 2005; Ohtani & Mukai, 2008; Raptis et al., 2024). These features are extended to BBFs, which similarly show an enhancement in B_z and $(-\mathbf{V} \times \mathbf{B})_y$ during storms. Our analysis shows that the sharp increase in $(-\mathbf{V} \times \mathbf{B})_y$ observed during the onset of BBFs (at the zero epoch) is primarily due to the change in velocity for both stormtime and non-stormtime BBFs (Figure 3b). While this holds true for all the BBFs, during geomagnetic storms BBFs are observed to have a more elevated convection electric field at the zero epoch and for a few minutes following that. This enhancement in flux transport during geomagnetic storms is the result of an elevated B_z in the plasma sheet. In other words, it is the plasma sheet conditions during geomagnetic storms that mainly drive the observed elevated flux transport during storms compared to non-stormtime, rather than a difference in the flow velocity or dipolarization of stormtime BBFs. The dipolarization after removing the mean background values, δB_z, does not differ significantly between stormtime and non-stormtime BBFs (Figure 1g). This suggests that the localized dipolarization may have a relatively greater influence during non-storm times and therefore the relative jump from the background plasma sheet values is larger during non-storm times compared to storm times (Table 1). Several factors should be considered when interpreting these results. The fastest BBFs may be undersampled, as their localized and transient nature means a spacecraft might only partially observe them, leading to an underestimation of their maximum velocity. Furthermore, our analysis does not separate BBFs by radial distance, a necessary step taken to ensure a sufficient number of events for statistical analysis during storms. Since BBFs evolve and decelerate as they propagate, the presented temporal profile is a composite picture of flows from various locations and evolutionary stages within the magnetotail plasma sheet.

While a drop in density and an increase in ion temperature are observed for non-stormtime BBF intervals (Figures 1d and 1e), a clear trend is not observed for stormtime BBFs. However, the recovery phase BBFs are observed to have a lower density and higher temperature compared to both non-stormtime and main phase BBF intervals. Our analysis shows that this could either be a feature of BBF intervals observed during HSS-driven storms or a result of dawn-dusk asymmetry of plasma sheet ion temperature during storms. HSS-driven storms are associated with a hotter plasma sheet (Denton et al., 2006). Studies have shown that during HSS-driven storms, the ion temperature in the plasma sheet increases during the recovery phase (Denton & Borovsky, 2008; Keesee et al., 2014). The higher ion temperature and lower density observed in the SEA of BBF intervals during recovery phase could be dominated by intervals associated with HSS-driven storms. A dawn-dusk asymmetry in plasma sheet ion temperature has been reported in several studies (e.g., Wang et al., 2012; Walsh et al., 2014 and references therein; Wing & Newell, 2002). The ion temperature variations observed in the SEA could also be influenced by the location of BBFs in either the dawn or dusk sectors. We investigated the dawn-dusk asymmetry

hypothesis by performing SEAs of both stormtime and non-stormtime events at dawn and dusk; however, the number of events after this additional binning was insufficient to support a statistically significant conclusion. Future work that includes additional data from other missions is required to identify the factors contributing to the increased ion temperature during the recovery phase observed in the superposed epoch analysis.

Although the general statistical properties of BBFs have been widely studied, this study is the first to investigate their characteristics during storms. Our analysis indicates that the behavior of BBFs during storms is strongly influenced by the stormtime plasma sheet conditions. ICME- and HSS-driven storms are associated with different plasma sheet dynamics (Denton et al., 2006). These distinct plasma sheet conditions could have an impact on the BBF characteristics. Examining BBFs in the context of both HSS- and ICME-driven storms will give insight into how different solar wind drivers influence BBF dynamics. Gabrielse et al. (2019) examined high-latitude mesoscale ionospheric flows and found that flows during ICME-driven storms are faster than those during HSS-driven storms. They also reported that main phase flows are faster than those during the recovery phase and non-storm periods. In our superposed epoch analysis, we observe enhancements in B_z and $(-\mathbf{V} \times \mathbf{B})_y$ during main phase BBF events, indicating that both B_z and velocity can contribute to moving more magnetic flux per unit width. However, in the ionosphere B_z doesn't change substantially, so only changes in velocity can contribute directly. However, the ionosphere flows are driven by the potential electric field of the magnetosphere flows, enabling enhancements in B_z in the magnetosphere to influence flows in the ionosphere. It would be interesting in future studies to more directly investigate whether these enhancements in ionospheric flow speeds may be associated with the elevated B_z and an enhancement of the convection electric field in the magnetosphere. Finally, a more detailed analysis that takes into account the radial distance of the identified BBFs from Earth and their distribution across the dawn–dusk sector is essential for a comprehensive understanding of their characteristics.

Conflict of Interest

The authors declare no conflicts of interest relevant to this study.

Data Availability Statement

Geotail magnetometer and plasma data are available through: https://darts.isas.jaxa.jp/app/stp/geotail/ascii.html. Storms and their characterization are available at Raptis (2025). The list of BBF intervals used for this analysis is available at Devanandan and Raptis (2025). The list of storms and associated solar wind drivers is available at Marchezi and Pinto (2025).

Acknowledgments
This research was supported by the NASA DRIVE Science Center for Geospace Storms (CGS) under Cooperative Agreement 80NSSC22M0163. SO acknowledges support by NSF Grant 2224986 and NASA Grant 80NSSC21K0036. The authors thank Jose Paulo Marchezi for providing us with the list of storms classified by storm type.

References

Angelopoulos, V., Baumjohann, W., Kennel, C. F., Coroniti, F. V., Kivelson, M. G., Pellat, R., et al. (1992). Bursty bulk flows in the inner central plasma sheet. *Journal of Geophysical Research*, *97*(A4), 4027–4039. https://doi.org/10.1029/91ja02701

Angelopoulos, V., Kennel, C. F., Coroniti, F. V., Pellat, R., Kivelson, M. G., Walker, R. J., et al. (1994). Statistical characteristics of bursty bulk flow events. *Journal of Geophysical Research*, *99*(A11), 21257–21280. https://doi.org/10.1029/94ja01263

Angelopoulos, V., Phan, T. D., Larson, D. E., Mozer, F. S., Lin, R. P., Tsuruda, K., et al. (1997). Magnetotail flow bursts: Association to global magnetospheric circulation, relationship to ionospheric activity and direct evidence for localization. *Geophysical Research Letters*, *24*(18), 2271–2274. https://doi.org/10.1029/97GL02355

Baumjohann, W., & Paschmann, G. (1990). Characteristics of high-speed ion flows in the plasma sheet. *Journal of Geophysical Research*, *95*(A4), 3801–3809. https://doi.org/10.1029/ja095ia04p03801

Denton, M. H., & Borovsky, J. E. (2008). Superposed epoch analysis of high-speed-stream effects at geosynchronous orbit: Hot plasma, cold plasma, and the solar wind. *Journal of Geophysical Research*, *113*(A7), A07216. https://doi.org/10.1029/2007ja012998

Denton, M. H., Borovsky, J. E., Skoug, R. M., Thomsen, M. F., Lavraud, B., Henderson, M. G., et al. (2006). Geomagnetic storms driven by ICME- and CIR-dominated solar wind. *Journal of Geophysical Research*, *111*(A7), A07S07. https://doi.org/10.1029/2005ja011436

Devanandan, A., & Raptis, S. (2025). List of BBFs from Geotail data (1994-2022) [Dataset]. *Zenodo*. https://doi.org/10.5281/zenodo.17902904

Fu, H. S., Khotyaintsev, Y. V., André, M., & Vaivads, A. (2011). Fermi and betatron acceleration of suprathermal electrons behind dipolarization fronts. *Geophysical Research Letters*, *38*(16), L16104. https://doi.org/10.1029/2011GL048528

Gabrielse, C., Pinto, V., Nishimura, Y., Lyons, L., Gallardo-Lacourt, B., & Deng, Y. (2019). Storm time mesoscale plasma flows in the nightside high-latitude ionosphere: A statistical survey of characteristics. *Geophysical Research Letters*, *46*(8), 4079–4088. https://doi.org/10.1029/2018GL081539

Hori, T., Lui, A. T. Y., Ohtani, S. C., Brandt, P., Mauk, B. H., McEntire, R. W., et al. (2005). Storm-time convection electric field in the near-Earth plasma sheet. *Journal of Geophysical Research*, *110*(A4), 2004JA010449. https://doi.org/10.1029/2004JA010449

Juusola, L., Østgaard, N., & Tanskanen, E. (2011). Statistics of plasma sheet convection. *Journal of Geophysical Research*, *116*(A8), A08201. https://doi.org/10.1029/2011JA016479

Kasaba, Y., Hayakawa, H., Ishisaka, K., Okada, T., Matsuoka, A., Mukai, T., & Takei, Y. (2006). Evaluation of DC electric field measurement by the double probe system aboard the Geotail spacecraft. *Advances in Space Research*, *37*(3), 604–609. https://doi.org/10.1016/j.asr.2005.05.006

Keesee, A., Elfritz, J., Fok, M.-C., McComas, D., & Scime, E. (2014). Superposed epoch analyses of ion temperatures during CME- and CIR/HSS-driven storms. *Journal of Atmospheric and Solar-Terrestrial Physics*, *115–116*, 67–78. https://doi.org/10.1016/j.jastp.2013.08.009

Marchezi, J. P., & Pinto, V. (2025). Catalog of geomagnetic storms, associated solar wind drivers (ICMES and HSSS), and the SYM-H intensity [Dataset]. *Zenodo*. https://doi.org/10.5281/zenodo.17967225

Merkin, V. G., Panov, E. V., Sorathia, K. A., & Ukhorskiy, A. Y. (2019). Contribution of bursty bulk flows to the global dipolarization of the magnetotail during an isolated substorm. *Journal of Geophysical Research: Space Physics*, *124*(11), 8647–8668. https://doi.org/10.1029/2019JA026872

Nakamura, R., Amm, O., Laakso, H., Draper, N. C., Lester, M., Grocott, A., et al. (2005). Localized fast flow disturbance observed in the plasma sheet and in the ionosphere. *Annales Geophysicae*, *23*(2), 553–566. https://doi.org/10.5194/angeo-23-553-2005

Nakamura, R., Baumjohann, W., Mouikis, C., Kistler, L., Runov, A., Volwerk, M., et al. (2005). Multi-point observation of the high-speed flows in the plasma sheet. *Advances in Space Research*, *36*(8), 1444–1447. https://doi.org/10.1016/j.asr.2005.05.101

Nishida, A. (1994). The Geotail mission. *Geophysical Research Letters*, *21*(25), 2871–2873. https://doi.org/10.1029/94GL01223

Ohtani, S., & Mukai, T. (2008). Statistical characteristics of the storm time plasma sheet. *Journal of Geophysical Research*, *113*(A1), 2007JA012547. https://doi.org/10.1029/2007JA012547

Ohtani, S., Shay, M. A., & Mukai, T. (2004). Temporal structure of the fast convective flow in the plasma sheet: Comparison between observations and two-fluid simulations. *Journal of Geophysical Research*, *109*(A3), 2003JA010002. https://doi.org/10.1029/2003JA010002

Pinto, V. A., Keesee, A. M., Coughlan, M., Mukundan, R., Johnson, J. W., Ngwira, C. M., & Connor, H. K. (2022). Revisiting the ground magnetic field perturbations challenge: A machine learning perspective. *Frontiers in Astronomy and Space Sciences*, *9*, 869740. https://doi.org/10.3389/fspas.2022.869740

Raptis, S. (2025). Geomagnetic storms—Classified—1993–2025 [Dataset]. *Zenodo*. https://doi.org/10.5281/zenodo.15127938

Raptis, S., Merkin, V., Ohtani, S., Gkioulidou, M., & Regoli, L. H. (2024). Plasma sheet magnetic flux transport during geomagnetic storms. *Geophysical Research Letters*, *51*(18), e2024GL110839. https://doi.org/10.1029/2024GL110839

Runov, A., Angelopoulos, V., Sitnov, M., Sergeev, V., Nakamura, R., Nishimura, Y., et al. (2011). Dipolarization fronts in the magnetotail plasma sheet. *Planetary and Space Science*, *59*(7), 517–525. https://doi.org/10.1016/j.pss.2010.06.006

Sciola, A., Merkin, V. G., Sorathia, K., Gkioulidou, M., Bao, S., Toffoletto, F., et al. (2023). The contribution of plasma sheet bubbles to stormtime ring current buildup and evolution of its energy composition. *Journal of Geophysical Research: Space Physics*, *128*(11), e2023JA031693. https://doi.org/10.1029/2023JA031693

Sitnov, M., Birn, J., Ferdousi, B., Gordeev, E., Khotyaintsev, Y., Merkin, V., et al. (2019). Explosive magnetotail activity. *Space Science Reviews*, *215*(4), 31. https://doi.org/10.1007/s11214-019-0599-5

Walsh, A. P., Haaland, S., Forsyth, C., Keesee, A. M., Kissinger, J., Li, K., et al. (2014). Dawn–dusk asymmetries in the coupled solar wind–magnetosphere–ionosphere system: A review. *Annales Geophysicae*, *32*(7), 705–737. https://doi.org/10.5194/angeo-32-705-2014

Wang, C., Gkioulidou, M., Lyons, L. R., & Angelopoulos, V. (2012). Spatial distributions of the ion to electron temperature ratio in the magnetosheath and plasma sheet. *Journal of Geophysical Research*, *117*(A8), A08215. https://doi.org/10.1029/2012ja017658

Wiltberger, M., Merkin, V., Lyon, J. G., & Ohtani, S. (2015). High-resolution global magnetohydrodynamic simulation of bursty bulk flows. *Journal of Geophysical Research: Space Physics*, *120*(6), 4555–4566. https://doi.org/10.1002/2015JA021080

Wing, S., & Newell, P. T. (2002). 2D plasma sheet ion density and temperature profiles for northward and southward IMF. *Geophysical Research Letters*, *29*(9), 21-1–21-4. https://doi.org/10.1029/2001gl013950

Yang, J., Toffoletto, F. R., Wolf, R. A., & Sazykin, S. (2015). On the contribution of plasma sheet bubbles to the storm time ring current. *Journal of Geophysical Research: Space Physics*, *120*(9), 7416–7432. https://doi.org/10.1002/2015JA021398